

SPARSE PARTIAL DERIVATIVES AND RECONSTRUCTION FROM PARTIAL FOURIER DATA

Elham Sakhaee and Alireza Entezari

CISE Department, University of Florida, Gainesville, FL

ABSTRACT

Signal reconstruction from the smallest possible Fourier measurements has been a key motivation in the compressed sensing research. We present an approach that exploits the interdependency and structural sparsity of partial derivatives for lowering the sampling rates necessary for accurate reconstruction. Our experiments show that for signals that are sparse in the gradient domain our proposed method significantly outperforms the existing approaches including the total variation (TV) based CS reconstruction.

Index Terms— Compressed Sensing, Partial Fourier, Total Variation, Gradient-domain Sparsity

1. INTRODUCTION

Signal reconstruction from the frequency domain samples is a classical problem in signal processing that has been widely studied [1, 2]. The problem arises in many sensing applications such as magnetic resonance imaging (MRI) and synthetic aperture radar [3]. Results in compressed sensing (CS) have established that accurate reconstruction from partial Fourier data is possible when the signal is sparse or that it can be represented sparsely in a transform domain [4]. Partial Fourier sensing and sparse reconstruction enable the reduction of the required number of measurements while maintaining the accuracy of signal reconstruction [5]. Principles of compressed sensing have been successfully applied in MR imaging where the reduction of acquisition time is all-important [6].

More generally for a linear sensing model, the reconstruction from partial data is formulated as a sparse solution to an under-determined system of linear equations [7]. Solving this under-determined system can be a well defined problem when we have incoherency between the sensing basis and the basis in which signal is sparsely represented [7]. While the Fourier and Dirac are the exemplar sensing and representation bases, natural images are often sparse in a transform domain. Wavelets have been shown to be effective in sparse representation of 1-D signals and their tensor-products have been used as sparsifying transforms for multidimensional signals

(e.g., images). Geometric transforms such as curvelets [8], ridgelets [9] and surfacelets [10] improve the sparse representation of multidimensional signals by adapting to the anisotropic structures in the signal. While geometric transforms improve the sparsity in representation, they are often redundant representations [11] and the redundancy factor impacts their effectiveness in practical reconstruction problems.

Another set of approaches to reconstruction from partial Fourier data rely on some form of sparsity in the gradient information [12, 5]. More specifically, the total variation (TV) methods regularize the solution to the under-determined system by penalizing the solutions with large variations. TV-based regularization methods are particularly effective for modeling images that are composed of homogeneous regions with transient edges [5]. For the class of piecewise constant signals the gradients exhibit more sparsity than the wavelet representations as the edges often appear as non-zero coefficients in multiple scales in the wavelet expansion. Therefore, the sparsity in the wavelet domain can be used together with TV for improving the image reconstruction [12, 13]. Finite-difference operators are a common choice for sparsification in the analysis model [14] and they appear naturally for piecewise constant signals in transform learning [15].

When either one of the partial derivatives are non-zero at a point, the TV model observes a non-zero variation; therefore, often the individual partial derivatives are sparser than the TV penalty image. The gradient-based reconstruction methods [3] leverage this increase in sparsity and reconstruct the partial (i.e., horizontal and vertical) derivatives individually and reconstruct the image based on the recovered partials.

Motivated by the gradient-based reconstruction methods [3], we propose a new formulation of the sparse approximation problem, from partial Fourier data, where all partial derivatives are simultaneously reconstructed. Effectiveness of this approach has been recently studied in the context of tomographic reconstruction from limited X-ray measurements in [16]. As discussed in Section 2, this formulation benefits from the interdependence of the partial derivatives and their structural sparsity to provide additional constraints that improve the accuracy of reconstruction. Experiments in Section 3 provide evidence that the proposed method significantly outperforms TV-based CS reconstruction for signals whose gradients are sparse.

This research was supported in part by the NSF grant CCF/CIF-1018149 and the ONR grant N00014-14-1-0762.

2. SPARSE APPROXIMATION OF PARTIAL DERIVATIVES

Let $\mathbf{f} \in \mathbb{R}^N$ denote an image with N pixels and \mathcal{F} be the 2-D Discrete Fourier Transform (DFT) restricted to a partial set of frequencies. The partial Fourier data \mathbf{p} , containing $n < N$ measurements, is obtained as $\mathbf{p} = \mathcal{F}\mathbf{f}$. Let \mathbf{D}_x and \mathbf{D}_y denote horizontal and vertical differential (difference) operators. For the image \mathbf{f} the partial derivatives are obtained by $\mathbf{f}_x = \mathbf{D}_x\mathbf{f}$ and $\mathbf{f}_y = \mathbf{D}_y\mathbf{f}$. The total variation-based CS reconstruction is the result of the following optimization problem:

$$\hat{\mathbf{f}} = \arg \min_{\mathbf{u} \in \mathbb{R}^N} \lambda \|\mathbf{u}\|_{BV} + \|\mathcal{F}\mathbf{u} - \mathbf{p}\|_2^2, \quad (1)$$

where \mathbf{u} is the optimization variable and $\|\mathbf{u}\|_{BV}$ is the total variation, defined as $\|\mathbf{D}_x\mathbf{u}\|_1 + \|\mathbf{D}_y\mathbf{u}\|_1$ [12]. The regularization parameter λ controls the sparsity of the gradient.

As discussed before, for a piecewise-constant image, the gradient magnitude image $\|\mathbf{f}\|_{BV}$, is often less sparse than \mathbf{f}_x or \mathbf{f}_y . Based on this observation the gradient-based image reconstruction method [3] reconstructs each of \mathbf{f}_x and \mathbf{f}_y individually in a sparse approximation framework by solving two separate convex problems:

$$\begin{aligned} \hat{\mathbf{f}}_x &= \arg \min_{\mathbf{u}_x \in \mathbb{R}^N} \lambda \|\mathbf{u}_x\|_1 + \|\mathcal{F}\mathbf{u}_x - \mathbf{p}_x\|_2^2 \\ \hat{\mathbf{f}}_y &= \arg \min_{\mathbf{u}_y \in \mathbb{R}^N} \lambda \|\mathbf{u}_y\|_1 + \|\mathcal{F}\mathbf{u}_y - \mathbf{p}_y\|_2^2, \end{aligned} \quad (2)$$

where $\mathbf{p}_x = \mathcal{F}\mathbf{D}_x\mathbf{f}$ and $\mathbf{p}_y = \mathcal{F}\mathbf{D}_y\mathbf{f}$ denote the partial Fourier data of the horizontal and vertical partial derivative images, obtained from \mathbf{p} via the Fourier multipliers of \mathbf{D}_x and \mathbf{D}_y as in [3]. These two problems approximate the gradient field of the underlying image by a vector field. However, as these problems are solved separately, the recovered vector field is not necessarily integrable and may not represent a valid gradient vector field. The post-processing approach presented in [3] is to obtain an integrable gradient vector field that approximates the nonintegrable recovered vector field from (2), in a least-squares sense.

In our approach we propose to solve the two sparse approximation problems simultaneously by exploiting the interdependence between the partial derivatives and incorporating the integrability constraint into the sparse approximation problem, rather than post-processing estimation as in [3]. The vector field $[\hat{\mathbf{f}}_x, \hat{\mathbf{f}}_y]^T$ corresponds to the gradient of a scalar field – the image – if it is curl-free (i.e., the gradient field is integrable and its integral along any closed curve is zero). Therefore, the partial derivatives can be tied with an additional zero-curl constraint at the sparse approximation stage:

$$\mathbf{D}_y\hat{\mathbf{f}}_x = \mathbf{D}_x\hat{\mathbf{f}}_y. \quad (3)$$

This constraint allows us to tie the two optimization problems

in (2) by penalizing solutions that exhibit non-zero curl:

$$\begin{aligned} \hat{\mathbf{f}}_x, \hat{\mathbf{f}}_y &= \arg \min_{\mathbf{u}_x, \mathbf{u}_y \in \mathbb{R}^N} \lambda (\|\mathbf{u}_x\|_1 + \|\mathbf{u}_y\|_1) + \|\mathcal{F}\mathbf{u}_x - \mathbf{p}_x\|_2^2 + \\ &\|\mathcal{F}\mathbf{u}_y - \mathbf{p}_y\|_2^2 + \gamma \|\mathbf{D}_y\mathbf{u}_x - \mathbf{D}_x\mathbf{u}_y\|_2^2. \end{aligned} \quad (4)$$

We define a new system matrix, \mathbf{G} , and denote the corresponding partial Fourier measurements from partial derivatives by \mathbf{p}' :

$$\mathbf{G} = \begin{bmatrix} \mathcal{F} & \mathbf{0} \\ \mathbf{0} & \mathcal{F} \\ \gamma\mathbf{D}_y & -\gamma\mathbf{D}_x \end{bmatrix}, \quad \mathbf{p}' = \begin{bmatrix} \mathbf{p}_x \\ \mathbf{p}_y \\ \mathbf{0} \end{bmatrix}.$$

Using the above definitions, the optimization problem in (4) can be formulated into an ℓ_1 regularized least squares problem over $2N$ variables:

$$[\hat{\mathbf{f}}_x, \hat{\mathbf{f}}_y]^T = \arg \min_{\mathbf{v} \in \mathbb{R}^{2N}} \lambda \|\mathbf{v}\|_1 + \|\mathbf{G}\mathbf{v} - \mathbf{p}'\|_2^2. \quad (5)$$

The severity of the penalty for non-zero curl in the solution to the sparse approximation problem is determined by the parameter γ that controls the fidelity of the solution versus the integrability constraint.

The two optimization problems in (2) involve $2N$ independent variables for which we have $2n$ (dependent) constraints given by \mathbf{p}_x and \mathbf{p}_y . In contrast the optimization problem in (5) has $2n + N$ constraints on $2N$ variables representing the horizontal and vertical partial derivatives. These additional N constraints help solve the sparse approximation problem more effectively allowing us to reduce the number of measurements n for a given sparsity rate of the signal.

The curl-free constraint becomes more effective in 3-D, where the reconstruction of the three partial derivatives (i.e., $\mathbf{f}_x, \mathbf{f}_y$ and \mathbf{f}_z) can be improved by three additional constraints: $\mathbf{D}_x\mathbf{f}_y = \mathbf{D}_y\mathbf{f}_x$, $\mathbf{D}_x\mathbf{f}_z = \mathbf{D}_z\mathbf{f}_x$ and $\mathbf{D}_z\mathbf{f}_y = \mathbf{D}_y\mathbf{f}_z$. For reconstruction of a volume composed of N voxels from n partial Fourier data, we can build an objective function, similar to (5), that has $3N$ variables for all partial derivatives, and $3n + 3N$ (dependent) constraints.

Several approaches exist for reconstructing the scalar-field (e.g. image) from its gradient data [17, 18, 19]. The image can be reconstructed by solving the Poisson equation:

$$\nabla^2 \hat{\mathbf{f}} = \mathbf{D}_x\hat{\mathbf{f}}_x + \mathbf{D}_y\hat{\mathbf{f}}_y, \quad (6)$$

where ∇^2 is the Laplacian operator. The Fourier expansion method [18] provides a solution that enforces integrability when the optimization in (5) leads to a residual curl from its fidelity term.

3. EXPERIMENTS

In our experiments we examine the effectiveness of image reconstruction in gradient domain through simultaneous recovery of partial derivatives with the curl-free constraint. Therefore we compare our method with total-variation-based (TV)

CS reconstruction [20] as well as individual recovery of partial derivatives (*GradRec*), from (2) as proposed in [3].

Similar to the experiments in [20, 3], the Fourier domain sampling is performed with a radial pattern and the sampling rate is defined as n/N . The regularization parameters in (5) are found empirically and set to $\lambda = 10^{-8}$ and $\gamma = 0.5$. For the methods *TV* and *GradRec* the best regularization parameters were selected to provide the most accurate reconstructions they can offer. The reconstruction accuracy is measured in terms of Signal to Noise Ratio (SNR) and reported in the logarithmic scale (dB).

The first set of experiments are carried out with Shepp-Logan phantom image of size 512×512 . The reconstructions are performed with only 2.5% of Fourier domain data, which is half of the sampling rate reported in [3]. Fig. 1 shows the results of gradient-based (*GradRec*) and *TV*-based (*TV*) CS reconstructions as well as proposed (*SPD*) method. This experiment suggests that when sampling rate is extremely low, *GradRec* does not return a faithful reconstruction and the curl-free constraint in *SPD* have a significant impact in the success of the sparse approximation. At this sampling rate *TV* image exhibits artifacts and poor recovery for the detailed features at the bottom.

The results demonstrate that, at such extremely low sampling rate, number of partial Fourier data is not enough for individual recovery of \hat{f}_x and \hat{f}_y as in *GradRec* method, and therefore projecting the recovered vector field onto an integrable vector field [3] can not compensate for imperfect recovery. In contrast, the simultaneous recovery of the partial derivatives, benefits from the additional 512×512 (dependent) zero-curl constraints and allows for near optimal reconstruction. Lack of enough samples also applies to the *TV* CS reconstruction, where 6599 Fourier samples are not enough for recovering 4386 non-zero pixels in the *TV* image (i.e., the image with magnitude of gradients in f).

The errors in reconstructions are shown in the last row of Fig. 1, where the intensities are amplified by a factor of 10 for illustration purposes. The error exhibited in reconstructions from *GradRec* and *TV* imply that curl-free constraint has a significant impact in reducing noise in homogeneous regions as well as artifacts along the edges.

Fig. 2 shows the reconstruction results for the Marschner-Lobb test function [21] limited to 2-D, quantized and sampled at 256×256 (top left). The reconstruction was performed from 18.5% of Fourier data. The images demonstrate the significant impact of integrating zero-curl knowledge at the sparse approximation stage. Strong artifacts are visible in reconstructions with *GradRec* and *TV* methods, while *SPD* recovers a nearly perfect image with 30.15 dB accuracy in terms of SNR. In this case, the 18.5% (12101) Fourier samples are not enough for the individual recovery of \hat{f}_x and \hat{f}_y each with 6172 non-zeros while the curl-free constraint in *SPD* enables accurate recovery. Similarly the *TV* CS reconstruction is unable to provide an accurate recovery as there are 10342 non-

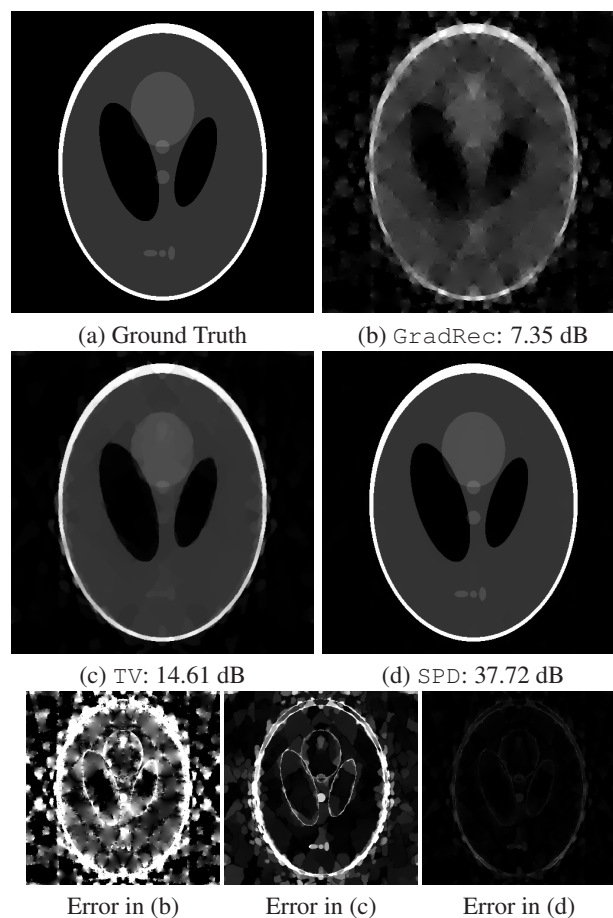


Fig. 1. Reconstruction of Shepp-Logan phantom from partial Fourier data at 2.5% sampling rate. The proposed *SPD* outperforms *TV* in recovering the details. The last row shows the errors in reconstruction (amplified by a factor of 10 for illustration purposes).

zeros in the *TV* image.

In the next set of experiments, the ground truth is a realistic analytical brain phantom of size 256×256 , developed in [22](Fig. 3(a)). The brain phantom carries detailed features and variations and effectively models real CT/MRI images. The reconstruction results for brain image with 17% of the Fourier data are shown in Fig. 3, which demonstrates the superiority of *SPD* method for recovery small features present in biomedical images [22]. While the SNRs are reported for the reconstruction of the entire image, Fig. 3(b,c, and d) show zoomed-in view of a portion of the image for comparison purposes. The last row in Fig. 3 shows the error images (amplified by a factor of 10 for illustration purposes) that highlight the artifacts present along the edges for *GradRec* and *TV* reconstructions while the proposed *SPD* method provides a near optimal recovery for sampling rates as low as 17%.

In order to compare reconstruction accuracy of the three methods as a function of sampling rate, SNR values for the

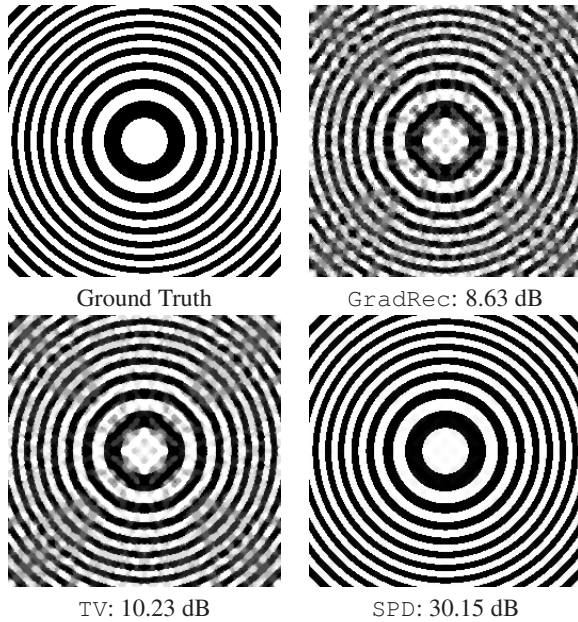


Fig. 2. The Marschner-Lobb dataset sampled at 256×256 , and recovered from 18.5% partial Fourier data.

Shepp-Logan and Brain experiments are plotted in Fig. 4. Expected by typical phase transition behaviour of ℓ_1 minimization problems [7], the graph in Fig. 4(a) shows that SPD is successful in finding the sparsest solution for the gradient vector field at lower sampling rates. This is attributed to the extra constraints that enable accurate recovery from convex optimization [7]. The plot also demonstrates that when enough samples are taken in Fourier space (e.g., 5%), both GradRec and SPD significantly outperform TV-based CS method – that agrees with the experiments in [3]. The transition to the near optimal recovery for the SPD method occurs at extremely low data rates (e.g., 2.5%). Fig. 4(b) shows this experiment for the brain dataset which also demonstrates that the phase transition occurs at lower sampling rates for the proposed SPD method compared to TV and GradRec.

It is worth noting that for images with non-sparse gradients (e.g., the Lenna images), where individual partial derivatives contain approximately as many non-zeros as the TV image, accuracy of SPD is similar to TV reconstruction, with no or little improvements.

4. CONCLUSION

In this paper, we propose a novel formulation for CS image reconstruction from incomplete Fourier data that exploits the interdependency of image partial derivatives to lower the necessary sampling rates for accurate recovery. Our formulation benefits from the integration of curl-free constraints into the sparse approximation problem. The experimental results show that at very low sampling rates (of Fourier data), the pro-

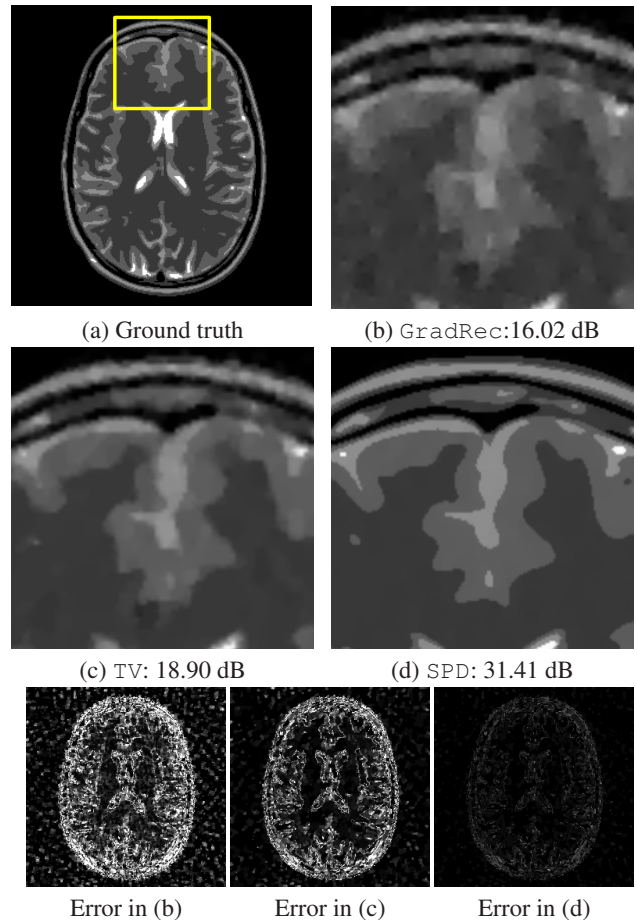


Fig. 3. Brain dataset recovered from partial Fourier data at a 17% sampling rate. Close-up views reveal near optimal recovery for the proposed SPD method. The last row are the corresponding error images which are amplified by a factor of 10 for illustration purposes.

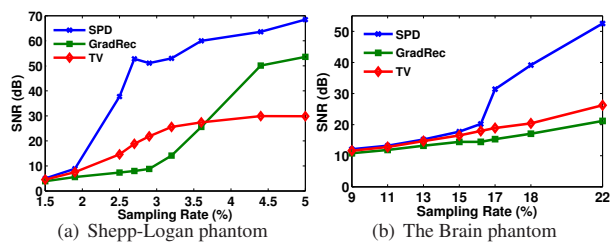


Fig. 4. Accuracy of reconstruction as a function of sampling rate. (a) In the Shepp-Logan dataset the proposed SPD approach achieves highly accurate solutions at 2.5%. (b) In the brain dataset this recovery occurs at 17% sampling rate.

posed approach achieves significantly higher accuracy, compared to existing methods that rely on the sparsity in the gradient information.

5. REFERENCES

- [1] Y. Bresler, M. Gastpar, and R. Venkataramani, "Image compression on-the-fly by universal sampling in fourier imaging systems," in *Proc. 1999 IEEE Information Theory Workshop on Detection, Estimation, Classification, and Imaging*, 1999, pp. 48–48.
- [2] M. Gastpar and Y. Bresler, "On the necessary density for spectrum-blind nonuniform sampling subject to quantization," in *Acoustics, Speech, and Signal Processing, 2000. ICASSP'00. Proceedings. 2000 IEEE International Conference on*. IEEE, 2000, vol. 1, pp. 348–351.
- [3] V. M. Patel, R. Maleh, A. C. Gilbert, and R. Chellappa, "Gradient-based image recovery methods from incomplete fourier measurements," *Image Processing, IEEE Transactions on*, vol. 21, no. 1, pp. 94–105, 2012.
- [4] D. Donoho, "Compressed sensing," *IEEE Transactions on Information Theory*, vol. 52, no. 4, pp. 1289–1306, 2006.
- [5] E. J. Candes, J. Romberg, and T. Tao, "Robust uncertainty principles: Exact signal reconstruction from highly incomplete frequency information," *IEEE Transactions on Information Theory*, vol. 52, no. 2, pp. 489–509, 2006.
- [6] M. Lustig, D. Donoho, J. Santos, and J. Pauly, "Compressed sensing mri," *Signal Processing Magazine, IEEE*, vol. 25, no. 2, pp. 72–82, march 2008.
- [7] A. M. Bruckstein, D. L. Donoho, and M. Elad, "From sparse solutions of systems of equations to sparse modeling of signals and images," *SIAM review*, vol. 51, no. 1, pp. 34–81, 2009.
- [8] E. Candès, L. Demanet, D. Donoho, and L. Ying, "Fast discrete curvelet transforms," *Multiscale Modeling & Simulation*, vol. 5, no. 3, pp. 861–899, Jan. 2006.
- [9] E. Candès and D. Donoho, "Ridgelets: A key to higher-dimensional intermittency?," *Philosophical Transactions of the Royal Society of London. Series A: Mathematical, Physical and Engineering Sciences*, vol. 357, no. 1760, pp. 2495–2509, 1999.
- [10] Y. M. Lu and M. N. Do, "Multidimensional directional filter banks and surfacelets," *Image Processing, IEEE Transactions on*, vol. 16, no. 4, pp. 918–931, 2007.
- [11] G. Kutyniok and D. Labate, *Shearlets: Multiscale Analysis for Multivariate Data*, Birkhauser Publication, first edition, 2012.
- [12] T. Goldstein and S. Osher, "The split bregman method for l1-regularized problems," *SIAM Journal on Imaging Sciences*, vol. 2, no. 2, pp. 323–343, 2009.
- [13] J. Yang, Y. Zhang, and W. Yin, "A fast alternating direction method for tvl1-l2 signal reconstruction from partial fourier data," *Selected Topics in Signal Processing, IEEE Journal of*, vol. 4, no. 2, pp. 288–297, 2010.
- [14] S. Nam, M. E. Davies, M. Elad, and R. Gribonval, "The cospase analysis model and algorithms," *Applied and Computational Harmonic Analysis*, vol. 34, no. 1, pp. 30–56, 2013.
- [15] S. Ravishankar and Y. Bresler, "Learning sparsifying transforms," *Signal Processing, IEEE Transactions on*, vol. 61, no. 5, pp. 1072–1086, 2013.
- [16] E. Sakhæe and A. Entezari, "Gradient-based sparse approximation for computed tomography," in *Proc. of Biomedical Imaging (ISBI), IEEE International Symposium on*, 2015, (to appear).
- [17] P. Pérez, M. Gangnet, and A. Blake, "Poisson image editing," in *ACM Transactions on Graphics (TOG)*. ACM, 2003, vol. 22, pp. 313–318.
- [18] R. T. Frankot and R. Chellappa, "A method for enforcing integrability in shape from shading algorithms," *Pattern Analysis and Machine Intelligence, IEEE Transactions on*, vol. 10, no. 4, pp. 439–451, 1988.
- [19] A. Agrawal, R. Raskar, and R. Chellappa, "What is the range of surface reconstructions from a gradient field?," in *Computer Vision—ECCV 2006*, pp. 578–591. Springer, 2006.
- [20] J. Bobin and S. Becker, "Nesta: A fast and accurate first-order method for sparse recovery," www-stat.stanford.edu/~candes/nesta/nesta.html, 2011.
- [21] S. R. Marschner and R. J. Lobb, "An evaluation of reconstruction filters for volume rendering," in *Proceedings of the conference on Visualization'94*. IEEE Computer Society Press, 1994, pp. 100–107.
- [22] M. Guerquin-Kern, L. Lejeune, K. P. Pruessmann, and M. Unser, "Realistic analytical phantoms for parallel magnetic resonance imaging," *Medical Imaging, IEEE Transactions on*, vol. 31, no. 3, pp. 626–636, 2012.